



Study the Effect of Laser Wavelength on ZnO Nanoparticle Characteristics Synthesized by Pulse Laser Ablation as an Antibacterial Application

Hadeel J. Imran^a , Kadhim A. Hubeatir^{a*} , Kadhim A. Aadim^b

^a Laser and Optoelectronics Engineering Dept., University of Technology-Iraq, Alsina'a street, 10066 Baghdad, Iraq.

^b Department of physics, College of Science, University of Baghdad, Baghdad, Iraq.

*Corresponding author Email: Kadhim.A.Hubeatir@uotechnology.edu.iq

HIGHLIGHTS

- Synthesis of ZnO nanoparticles was performed using PLAL with different wavelengths
- The study and characterization of the ZnO nanoparticle were achieved.
- The antibacterial activity of ZnO was studied on coli and S. aurous.
- The nanomaterials were proved to have good biocompatibility and antibacterial properties.

ARTICLE INFO

Handling editor: Evan T. Salim

Keywords:

PLAL; NPs; Zinc Oxide (ZnO); Wavelength; Laser.

ABSTRACT

In recent years, biologists, chemists, materials scientists, and engineers have become interested in Nano-sized particles because of their unique properties. In this paper, ZnO nanoparticles were synthesized using an Nd: YAG laser with 800 mJ at 1064 nm and 532 nm (the fundamental and second harmonic wavelengths). The characteristics of optical, morphological, structural, wettability and antibacterial activity have been studied. The used technique of PLAL was successful in nanoparticle formation. It was proved in color changes, which was an indication of ZnO nanoparticle formation. The optical measurements show a decrease in absorption wavelength and an increase in the band gap, an indication of the formation of quantum confinement due to nanoparticle formation. The XRD involves the formation of polycrystalline ZnO at both wavelengths. Also, the FE-SEM proved the formation of nanoparticles with a semispherical shape and little agglomeration on the surface. However, the EDX shows Zn and O in the film, which means the formation of ZnO. The low contact angle indicates high wettability, which means that the material has high biocompatibility. Finally, the antibacterial test was done on two types of bacteria (E. coli and S. aurous) and showed an antibacterial effect on both types with different NP concentrations.

1. Introduction

The growing resistance of microbial organisms to multiple antibiotics, combined with the continued emphasis on healthcare costs, has prompted researchers to create new antimicrobial substances that are effective against drug resistance [1]. Metal nanoparticles' antibacterial activity has been linked to their small size and high surface-to-volume ratio, encouraging them to interact directly with microbial membranes rather than simply because metal ions are released through solutions [2,3]. Zinc oxide nanoparticles (ZnO NPs) have piqued the interest of researchers due to their intriguing physical and chemical properties [4,5]. Because of its optical, electronic, and electrical properties, ZnO, one of the promising semiconductor materials from group II-VI, has gained a lot of attention in many fields, especially in nanoscale form, such as gas sensing, optoelectronics, photocatalysis, and biosensors [6]. ZnO NPs have been used as antimicrobial agents due to their efficacy in pathogen-resistant strains, low toxicity, and heat resistance [7,8].

Pulsed Laser Ablation in Liquids (PLAL) has recently emerged as the most common and efficient method for this purpose [9]. This is due to its simplicity, effectiveness, ease of experimental setup, high purity (free of surface contamination), and the low number of chemical species required for production [10]. This technique uses high-intensity short pulses up to a nanosecond from an infrared laser source in the focusing condition to produce a tiny particle with unique properties in the nanoscale form via laser-matter interaction [11,12].

Previous research on the use of laser ablation to assist in synthesizing ZnO nanostructured materials revealed that: Ismail et al. produced and characterized colloidal ZnO nanoparticles in water using nanosecond laser ablation [13]. Hu et al. studied the effect of target and liquid media on the morphologies of ZnO nanoparticles prepared by laser ablation in solution [14]. Honda et al. successfully synthesized ZnO nanorods by ablating Zn in liquid media with a millisecond laser. They investigated the effect of varying the pulse width and peak power on particle size [4]. Ayman M. Mostafa studied the ZnO/PVA nanocomposite synthesized by pulsed laser ablation of zinc dust target immersed in the PVA solution carried out by Nd: YAG laser [15]. Khashan et al. studied the Antibacterial activity of Zinc Oxide nanostructured materials synthesis by laser ablation method [8].

In this work, Zinc oxide nanoparticles have been prepared by ablating a Zinc solid target in distilled water by two wavelengths, 1064nm, and 532 nm. Several techniques investigated the physicochemical properties of the prepared samples as UV–vis spectroscopy, FE-SEM, EDX, XRD, and contact angle. In addition, the antibacterial activity was examined for prepared colloidal on two different bacteria, *Staphylococcus aureus* (a Gram-positive bacterium) and *Escherichia coli* (a Gram-negative bacterium). This way, a higher density of spherically shaped nanoparticles with small diameters has been obtained using 1064 nm wavelength for ablation times up to 10 min.

2. Material and Method

2.1 Material and Preparation of ZnO Nanoparticles

The solid Zinc target (99.99% purity) with dimension 1 cm * 1 cm and distilled water distilled with Millipore water purification system. Zn pellet's laser ablation in distilled water produced Zinc oxide nanoparticles. The pellet immersed in a glass vessel contained deionized water. The water height above the target was adjusted to be around 8 mm. The laser ablation process was carried out using Nd-YAG operating at 1064 nm and 532 nm. The laser energy used for the ablation was 800 mJ at a 6 Hz repetition frequency. The laser beam was focused on the Zn pellet using the positive lens with a focal length of 9 cm, and the spot size was 2.5 mm. to carry out the laser ablation, as shown in Figure 1.

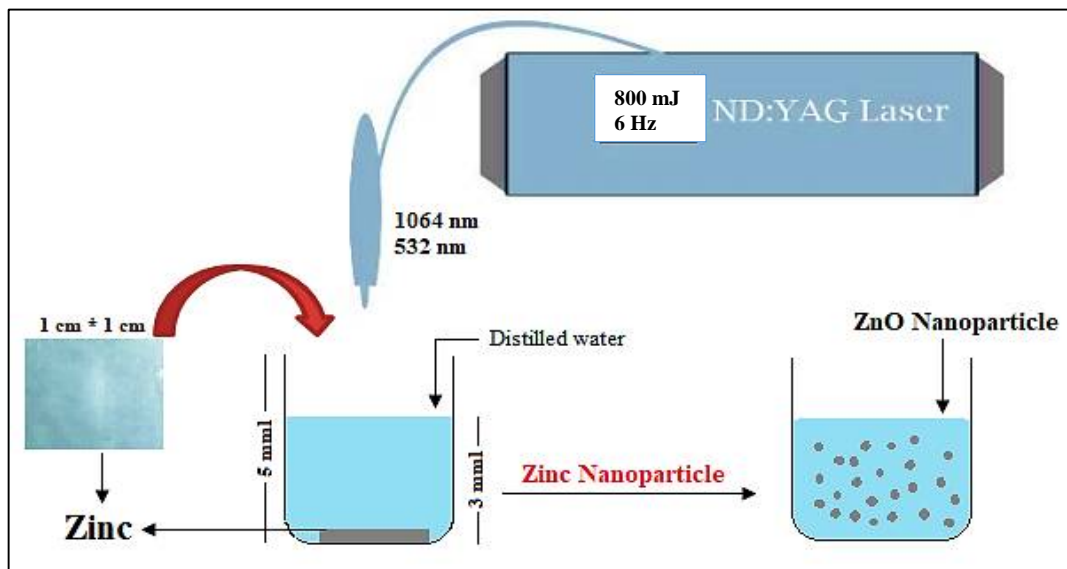


Figure 1: The schematic diagram of the experimental work

2.2 Characterization of ZnO Nanoparticles

The crystal structure of the synthesized ZnO nanoparticle was performed by X-ray diffraction (XRD) using PANalytical X Pert Pro target Cu-K α ($\lambda=0.1540$ nm), the tube operated at 45 kV, the scan was collected over a 2θ range of 20-70 $^\circ$. The grain size was determined using Debye–Scherrer equation [16]:

$$D = (k\lambda) / (\beta \cos\alpha) \quad (1)$$

Where k is 0.9, the Scherrer constant, λ is the X-ray constant (0.15406 nm), D is the average crystal size, β is the full width half maximum (FWHM), and α is Bragg's angle [17]. The UV–Vis spectrophotometer model (Metertech, SP8001 spectrophotometer, Japan) in the range of 100-1000 nm was used for optical properties measurement. The nanoparticle concentration in the colloidal was measured using Atomic Absorption Spectrometry (AAS). The surface morphology, particle size, and chemical composition of prepared nanoparticles were examined using field emission scan electron microscopy (FE-SEM), which was conducted using JSM-IT800 (origin) equipped with energy dispersive X-ray EDX.

2.3 Anti-Bacterial Activity Assay of ZnO Nanoparticles

The antibacterial activity of ZnO NPs was examined against two clinical isolates, *Escherichia coli* (Gram-negative) and *Staphylococcus aureus* (gram-positive). The stock cultures for these two bacterial isolates were transferred into Mueller Hinton agar medium, incubated overnight at 37 $^\circ$ C, and stored in the refrigerator at 4 $^\circ$ C until used. The antibacterial activity of ZnO

NPs was inspected using a good dissemination procedure. First, Wells with diameters of about 6 mm were made at the surface of agar media by tips of the micropipette, then NPS suspensions with different concentrations. These plates were kept in the incubator for 24 h. The antibacterial effectiveness of ZnO NPs was recorded by measuring inhibition zone diameters from different directions using a ruler more than once. All tests were duplicated, and purified water was utilized as an adverse control treatment [18].

3. Results and Discussion

The used technique of PLAL succeeded in nanoparticle formation. It was proved in color changes, indicating ZnO nanoparticle formation. Figure 2 shows the colloidal prepared by 532 nm with yellow and the other with 1064 nm has a white color. The concentration of each colloidal was measured using Atomic Absorption Spectrometry (AAS), illustrated in Table 1. Where the colloidal prepared with 532 nm wavelength have 102 $\mu\text{g ml}^{-1}$ concentration and colloidal prepared with 1064 nm have 81 $\mu\text{g ml}^{-1}$ concentration, this result coincides with the color of colloidal where the first have higher ZnO particle. More noticed darker color (yellow) while the other has lower concentration and Light color (white). This behavior was also noticed in [19]. The 532 nm was less affected by water and had more energy than the 1064 nm. The wavelength was inversely proportional to energy, so it absorbed more particles from the target surface. The most important reason for this concentration difference is that the shorter wavelength, the larger the optical absorption [20]. When more energy is supplied to the target, a more intense plasma plume is produced, which in turn causes a greater amount of material to be ablated, increasing the nano-colloid's density. These results were for two samples of the same power (800 mJ) and time of exposure (10 min) to the laser.



Figure 2: The colloidal suspension of ZnO nanoparticle prepared by PLAL technique

Table 1: The concentration of ZnO nanoparticle in the colloidal

	Wavelength (nm)	Energy (mJ)	Concentration ($\mu\text{g ml}^{-1}$)
ZnO	1064	800	81
ZnO	532	800	102

The optical absorption was measured using UV–Vis spectroscopy for the synthesized nanoparticle, shown in Figure 3. The absorption peak for ZnO NPs prepared at 1064 nm ranged from 190-230 nm to 220-255 nm for the sample prepared at 532 nm. It could be noticed that each sample has a blue shift as compared with bulk ZnO (365) due to the quantum confinement, which confirms the formation of NPs in the colloidal [21]. The NPs prepared with 532 nm have a higher peak because they have high NPs concentration, which increases the absorption peak. More particle concentration means more absorption.

Furthermore, the energy band gap for the prepared sample was calculated from the extrapolation of $h\nu$ vs. $(\alpha h\nu)^2$ curve. The band gap value was obtained by drawing a straight line on the curve intersecting with $h\nu$ at the X-axis. Figure 4 shows the band gap of prepared ZnO, which exhibits higher band gap energy. As expected, the smaller part size has a higher band gap, where it was 4.10 eV in 532 nm and 3.89 eV in 1064 nm, indicating that the particle formed with 532 nm was smaller than that formed with 1064 nm. This result is consistent with Ref [10].

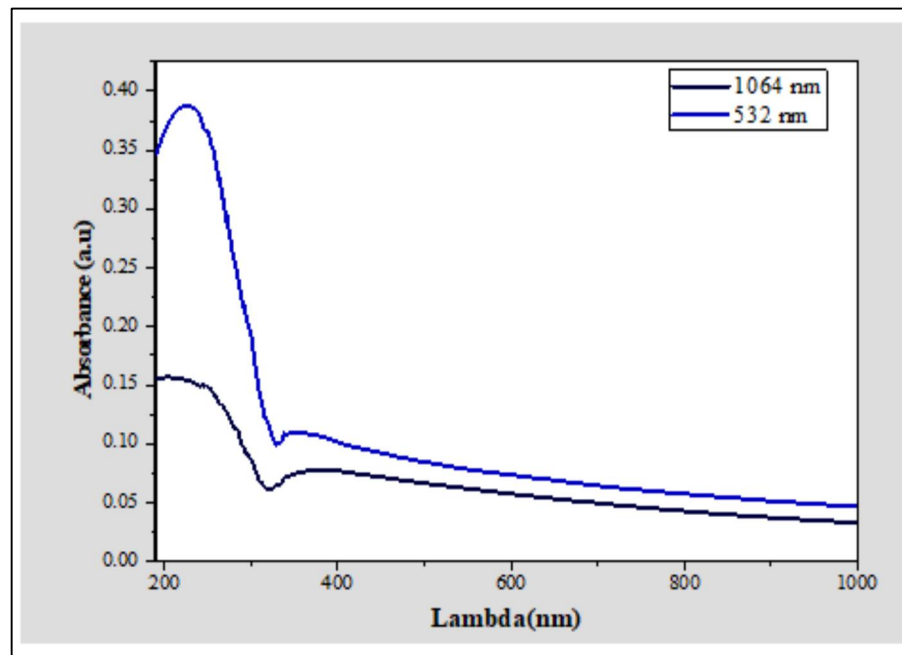


Figure 3: UV-vis absorption spectrum of the ZnO nanoparticle prepared by PLAL

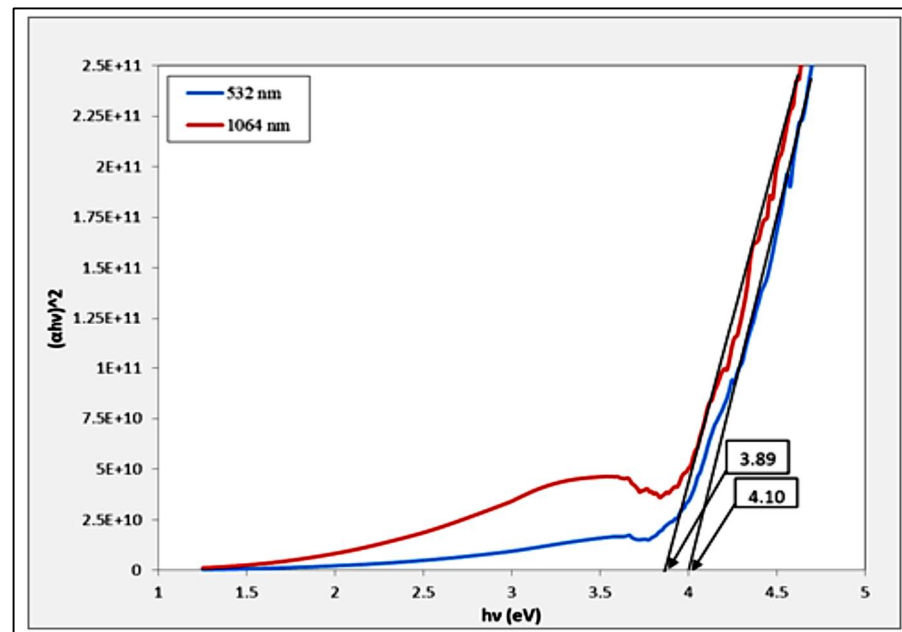


Figure 4: Energy band gap determination for ZnO nanoparticle

The synthesized zinc oxide nanoparticles' structure and degree of crystallinity were investigated using XRD. Figure 5 shows the XRD pattern of ZnO nanoparticles prepared at 1064 and 532nm. For 1064 nm, the XRD peak is located at $2\theta = 31.8, 36.4, 47.8$ and 63.2° indexed as (100), (101), (102), and (103). On the other hand, in the ZnO film prepared at 532 nm, the observed peak is $2\theta = 31.4, 34.4, 36.2, 47.4,$ and 62.8° indexed as (100), (002), (101), (102) and (103). These patterns are in good agreement with standard card (96-230-0451). This result indicates that the film has a polycrystalline and hexagonal wurtzite structure. Furthermore, it could be noticed that both samples have nearly the same peak intensity. Still, the sample prepared with 532 nm has a diffraction pattern that appeared at 34.4 , which was (002) due to having a higher concentration of ZnO NPs than that prepared with 1064 nm, so there are more particles oriented in a hexagonal wurtzite structure. Table 2 indicates the lattice parameter, FWHM, and the sample's average crystal size (D).

The XRD information for both samples was listed in Table 2, including the 2θ , FWHM, Crystalline size (nm), hkl, average crystal size, and card number. According to the table and Equation 1, the FWHM was inversely proportional to crystal size. Also, it was noticeable that there are a decrease in FWHM in the sample prepared with 1064 nm with little increase in the peak intensity and crystal size, which mean crystallinity improvement as the ZnO concentration increase in the colloidal. This result is in accordance with previous research [22].

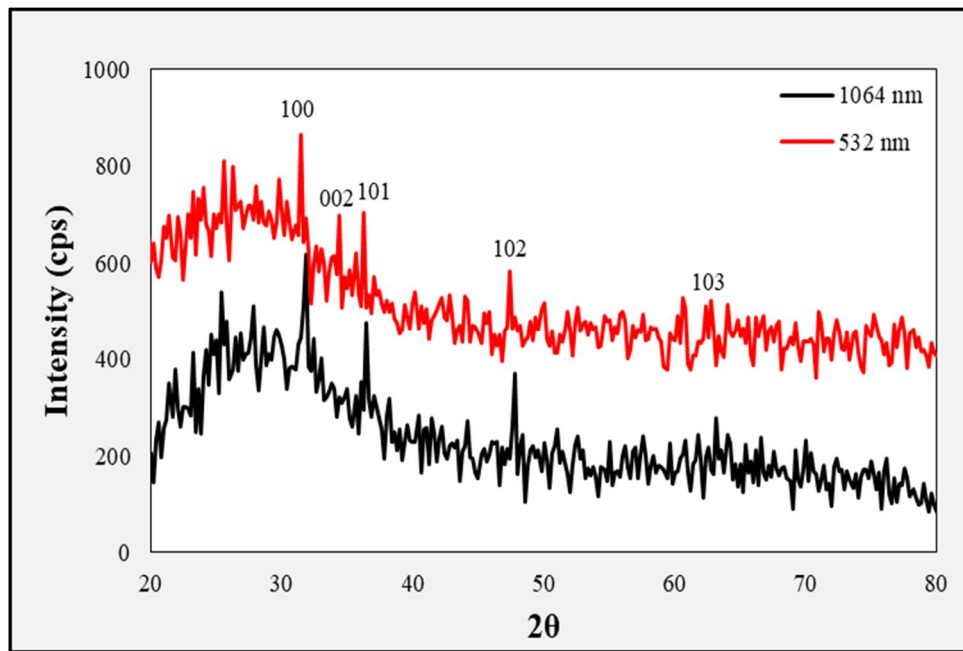


Figure 5: The XRD patterns of each ZnO colloidal prepared via PLAL

Table 2: The lattice parameter of ZnO crystal

Wavelength(nm)	2θ (°)	FWHM (Degree)	Crystalline size (nm)	(hkl)	Average C.S (nm)	Card No.
532	31.4	0.91	9.0799	100	30.544	96-230-0451
	34.4	0.45	18.504	002		96-230-0451
	36.2	0.18	46.492	101		96-230-0451
	47.4	0.21	41.367	102		96-230-0451
	62.8	0.25	37.277	103		96-230-0451
1064	31.8	0.21	39.385	100	36.256	96-230-0451
	36.4	0.4	20.934	101		96-230-0451
	47.8	0.19	45.792	102		96-230-0451
	63.2	0.24	38.914	103		96-230-0451

The morphological structure, grain size, and shape of ZnO nanoparticles were analyzed using Field Emission Scan Electron Microscopy (FE-SEM), which EDX supplemented to obtain the chemical composition. Figures 6(A) and 7(A) show the surface morphology for the sample prepared with 1064 nm and 532 nm, respectively. The surface was covered by uniform and a small particle but had a little aggregation. Although Figures 6(B) and 7(B) show the histogram graph for the particle distribution, indicating that nanoparticles synthesized at 1064 nm were about 10- 60 nm in diameter, and the normal particle was around 30 nm. While at 532 nm, the synthesized nanoparticle has a diameter of about 15-40 nm, and the normal particle size was 25 nm. There is a little difference in particles due to little difference in NPs concentration. Each wavelength for the preparation of nanoparticles has shown a well-defined particle-like morphology with a plenitude of spherical shape particles, which was preferred for antibacterial application.

The EDX result showed that the thin film contained oxygen and zinc, which means that the film was ZnO. Also, the EDX result proved that at 352 nm wavelength, the concentration of ZnO is higher than at 1064 nm, observed from the peak intensity in Figures 8 (A and B). This is because all the other elements emitted in the EDX figure are for the substrate, which is glass.

In vitro wettability of biomaterials is assessed using the contact angle (CA) at the liquid-solid interface. A high CA or high fluid-solid adhesion indicates a hydrophobic solid surface or low wettability. A low CA indicates a high wettability or hydrophilic surface, which means a continuous fluid film over the solid surface. Three forces influence a solid substrate's wettability: the solid's surface tension, the liquid's surface tension, and the interfacial tension [23]. Figure 9 (A and B) shows the prepared colloidal's contact angle, which seems to be between 21.76 and 23.47 for ZnO synthesized with 1064 nm and between 23.07 and 22.61 for ZnO synthesized with 532 nm. Both samples seem to have nearly the same CA value because there is not much difference between them in concentration. This means that the nanoparticle in colloidal have less interfacial tension, decreasing the CA and increasing the wettability on the surface. The CA of the two samples indicated that the material has high biocompatibility because it has high wettability, which was one of the most important biomaterial characteristics. Finally, the higher wettability means a larger area covered with colloidal, which means a high antibacterial effect.

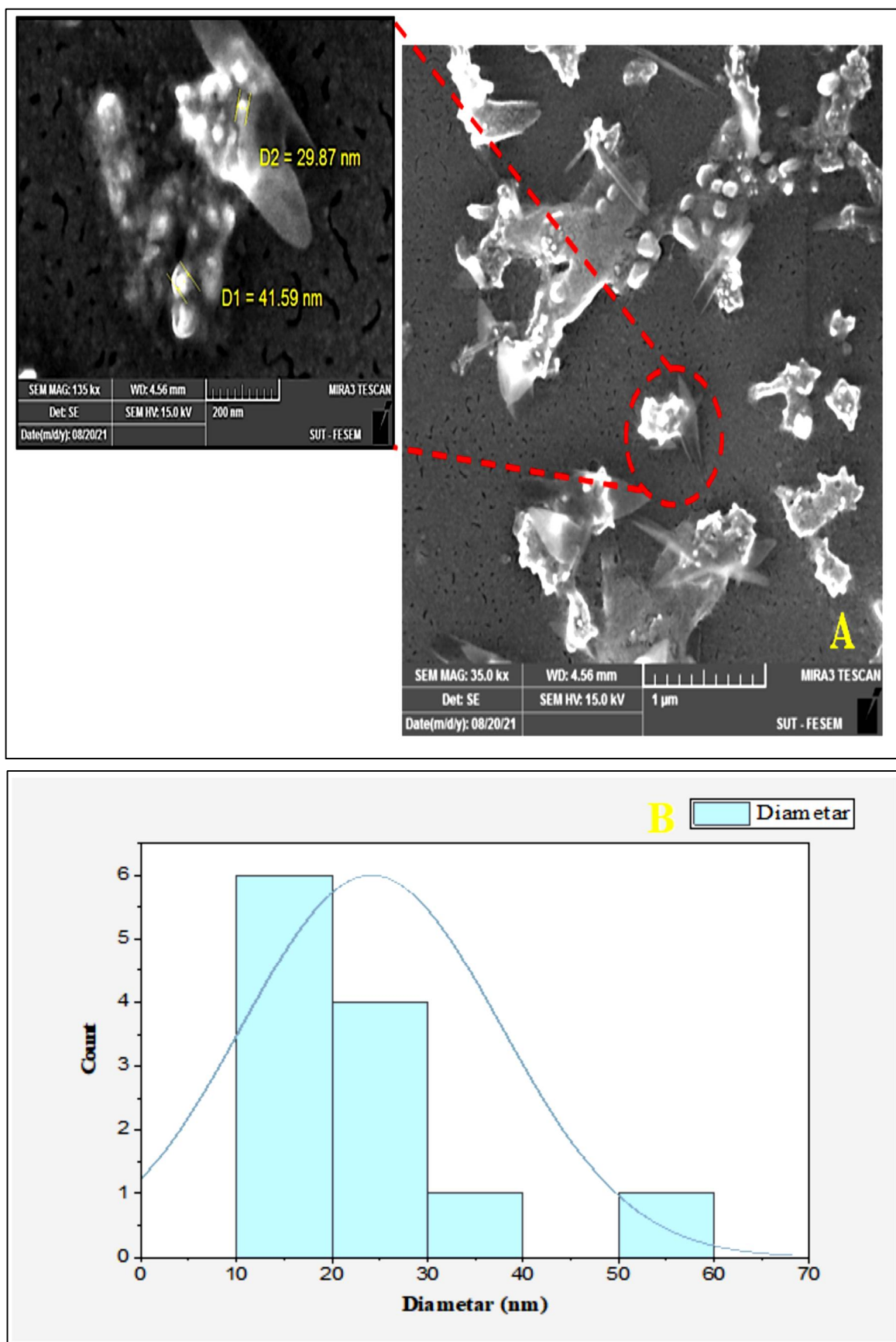


Figure 6: FE-SEM image of ZnO film prepared by 1064 nm laser wavelength, A) is the image at 200 nm amplification, B) is the histogram of particle diameter

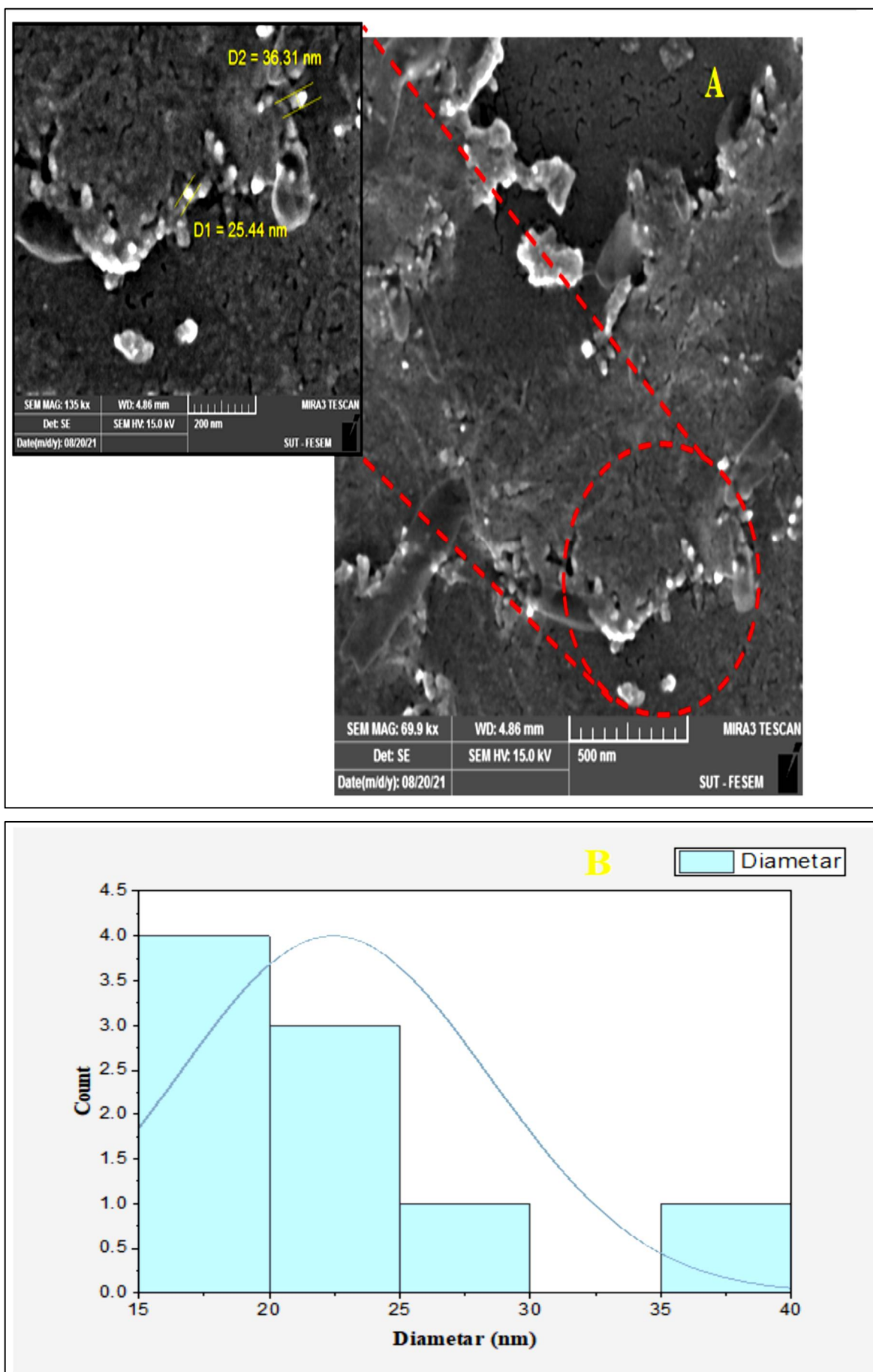


Figure 7: FE-SEM image of ZnO film prepared by 1064 nm laser wavelength, a) is the image at 200 nm amplification, b) is the histogram of particle diameter

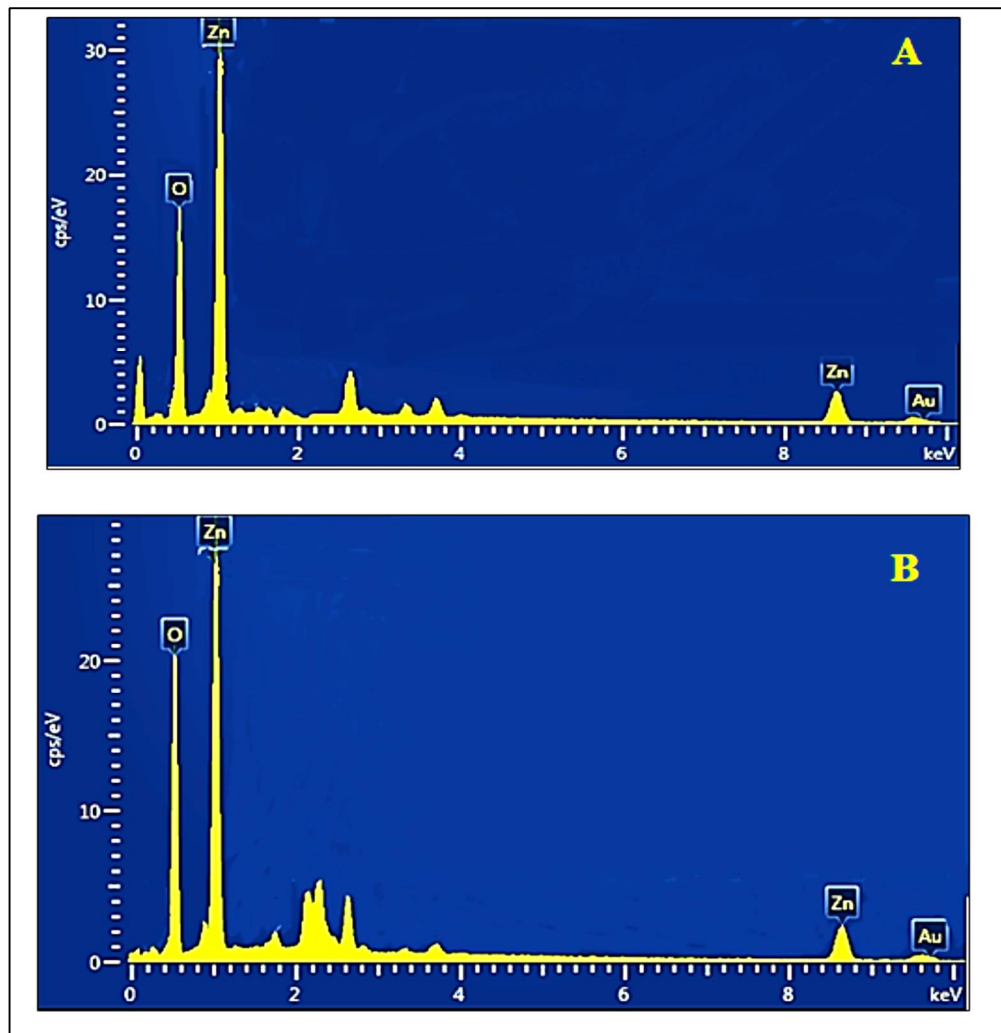


Figure 8: The EDX result of ZnO nanoparticle (a) prepared at 1064 nm, (b) prepared at 532 nm

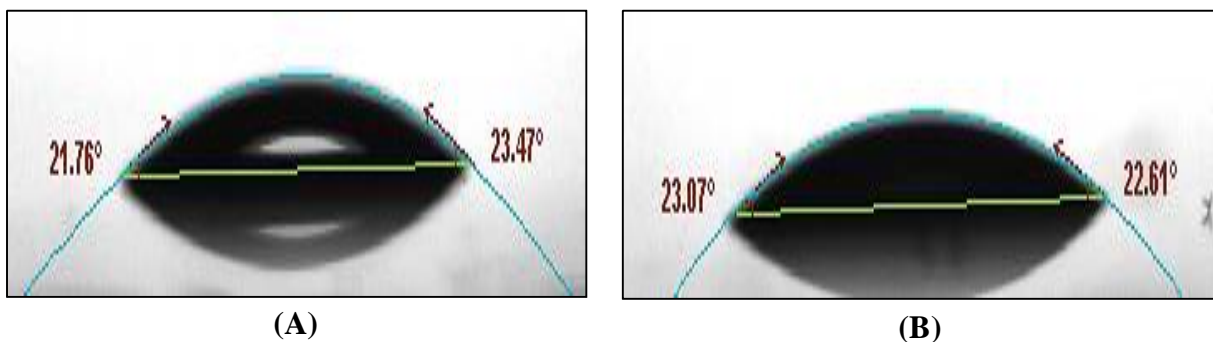
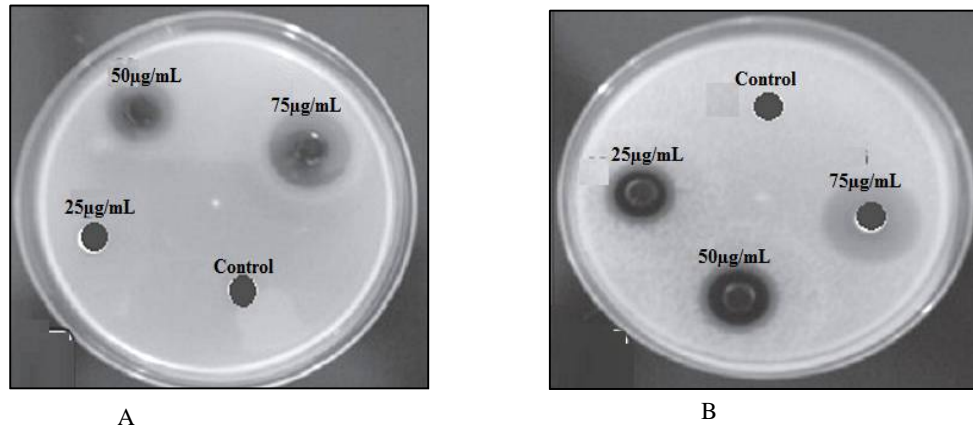
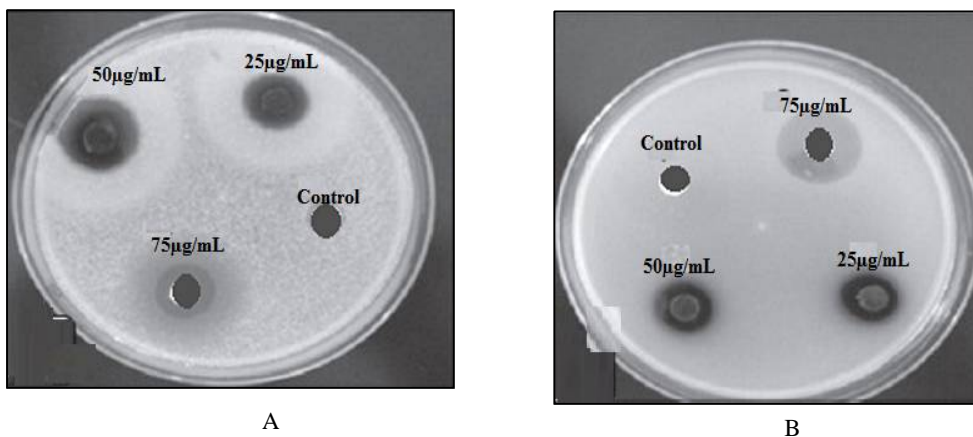


Figure 9: Contact angle image of the prepared ZnO at the wavelength (a) 1064 nm, (b) 532 nm

The antibacterial activity has been done using the good diffusion method on two types of bacteria, *Escherichia coli* (*E. coli*) and *Staphylococcus aureus* (*S. aureus*). For each sample, have three times mitigation (25, 50 and 75 $\mu\text{g/mL}$) to indicate how the NPs concentration will affect the bacteria. Figure 10 (A and B) show the antibacterial effect of ZnO NPs prepared at 1064 nm, and Figure 11 (A and B) for ZnO NPs prepared at 532 nm. It could be noticed that each sample has a clear circle arrowed it, which was a clear zone that shows how much the NPs affect the bacteria. There is a calling zone for all samples, and it was increased with increasing NPs concentration. The calling for the sample prepared with 532 nm is a little larger than that prepared with 1064 nm due to higher concentration and small particle size, leading to more bacteria. The clear zone was measured and listed in Table 3.

Table 3: The value of the clear zone for both samples and each bacteria on different mitigation

Concentration $\mu\text{g/mL}$	Escherichia coli		Staphylococcus aureus	
	1064nm	532nm	1064nm	532nm
0.0	0.0	0.0	0.0	0.0
25	8.2	6.6	7.4	7.2
50	10.5	9.9	10.3	9.2
75	13.9	12.6	13.4	12.4

**Figure 10:** Effect of ZnO NPs prepared with 1064 nm in *S. aureus* growth curve and *E. coli* growth curve**Figure 11:** Effect of ZnO NPs prepared with 532 nm in *S. aureus* growth curve and *E. coli* growth curve

4. Conclusion

The ZnO nanoparticle was successfully synthesized using the solid-state Nd: YAG laser at 1064 nm and 532 nm using the PLAL technique. The UV-Vis spectroscopy indicates that the energy band gap has a blue shift in both samples, which means the quantum confinement due to the NPs formation. While the XRD investigates the formation of the ZnO structure and the sample prepared with 532 nm has a pattern (002), it does not appear in the sample prepared with 1064 due to the high concentration, which leads to the appearance of more peaks from the material. The FE-SEM proved the formation of nanoparticles in a size range between (10-60) at 1064 nm preparation and (15-40) at 532 nm. Also, show the shape, which has a semispherical particle, and the surface was covered by uniform but had a little aggregation in both wavelengths. The EDX result proved that the material contained (Zn) and (O), which indicate the ZnO formation, and at 352 nm wavelength, the concentration of ZnO is higher than at 1064 nm, which was observed from the peak intensity. Each prepared NP shows a lower CA, which means high wettability, indicating that the material had high biocompatibility because it had high wettability, which was one of the most important biomaterial characteristics. The higher wettability means a larger area covered with colloidal and a high antibacterial effect. The antibacterial effect has been proved using different concentrations of NPs against two types of bacteria (*E. coli* and *S. aureus*).

Acknowledgment

This work was supported by the University of Technology, Iraq. We would also like to acknowledge the University of Baghdad for supplying this study's necessary equipment and devices.

Author Contribution

Hadeel J. Imran and Kadhim A. Aadim; methodology, resources, investigation, Hadeel J. Imran; software, formal analysis, data curation, writing—original draft preparation, Kadhim A. Hubeatir; writing—review and editing, Kadhim A. Hubeatir and Kadhim A. Aadim; supervision, project administration. All authors have read and agreed to the published version of the manuscript.

Funding

This research received no specific grant from any funding agency in the public, commercial, or not-for-profit sectors.

Data availability statement

The data that support the findings of this study are available on request from the corresponding author.

Conflicts of interest

The authors declare that there is no conflict of interest.

References

- [1] A. J. Bohan, E. Alhtheal, K. S. Shaker, A. Jabbar Bohan, K. Salim Shaker, Synthesis Nano Zinc Oxide Materials and Their Activity on Fungus Growth, *Eng. Technol. J.*, 35 (2017) 76–84.
- [2] A. A. Menazea, Antibacterial activity of TiO₂ doped ZnO composite synthesized via laser ablation route for antimicrobial application, *J. Mater. Res. Technol.*, 9 (2020) 9434–9441. <https://doi.org/10.1016/j.jmrt.2020.05.103>
- [3] U. M. Nayef, K. A. Hubeatir, Z. J. Abdulkareem, Characterisation of TiO₂ nanoparticles on porous silicon for optoelectronics application, *Mater. Technol.*, 31 (2016) 884–889. <https://doi.org/10.1080/10667857.2015.1132988>
- [4] M. Honda et al., ZnO nanorods prepared: Via ablation of Zn with millisecond laser in liquid media, *Phys. Chem. Chem. Phys.*, 18 (2016) 23628–23637. <https://doi.org/10.1039/c6cp04556a>
- [5] U. M. Nayef, K. A. Hubeatir, Z. J. Abdulkareem, Ultraviolet photodetector based on TiO₂ nanoparticles/porous silicon heterojunction, *Optik*, 127 (2016) 2806–2810. <https://doi.org/10.1016/j.ijleo.2015.12.002>
- [6] A. Kolodziejczak-Radzimska, T. Jesionowski, Zinc oxide—from synthesis to application: A review, *Materials*, 7 (2014) 2833–2881. <https://doi.org/10.3390/ma7042833>
- [7] W. Chen et al., ZnO colloids, ZnO nanoparticles synthesized by pulsed laser ablation of zinc powders in water, *Mater. Sci. Semicond. Process.*, 109 (2020) 104918. <https://doi.org/10.1016/j.mssp.2020.104918>
- [8] K. S. Khashan, B. A. Badr, G. M. Sulaiman, M. S. Jabir, S. A. Hussain, Antibacterial activity of Zinc Oxide nanostructured materials synthesis by laser ablation method, *J. Phys. Conf. Ser.*, 1795 (2021) 1–5. <https://doi.org/10.1088/1742-6596/1795/1/012040>
- [9] H. J. Imran, K. A. Hubeatir, K. A. Aadim, and D. S. Abd, Preparation Methods and Classification Study of Nanomaterial: A Review, in *Iraqi Academics Syndicate International Conference for Pure and Applied Sciences (IICPS)*, 1818, 2021, 12127. <https://doi.org/10.1088/1742-6596/1818/1/012127>
- [10] S. I. Al-Nassar, F. I. Hussein, and A. K. Ma, The effect of laser pulse energy on ZnO nanoparticles formation by liquid phase pulsed laser ablation, *J. Mater. Res. Technol.*, 8 (2019) 4026–4031. <https://doi.org/10.1016/j.jmrt.2019.07.012>
- [11] A. M. Mostafa and E. A. Mwafy, Synthesis of ZnO and Au@ZnO core/shell nano-catalysts by pulsed laser ablation in different liquid media, *J. Mater. Res. Technol.*, 9 (2020) 3241–3248. <https://doi.org/10.1016/j.jmrt.2020.01.071>
- [12] K. A. Aadim, R. H. Jassem, B. H. Adil, M. M. Farhan, S. M. Al-Chalabi, Synthesis of zinc nanoparticles by laser induced plasma and its effects on levels of thyroid hormones, *AIP Conf. Proc.*, 2307, 2020, 1–7. <https://doi.org/10.1063/5.0032721>
- [13] R. A. Ismail, A. K. Ali, M. M. Ismail, K. I. Hassoon, Preparation and characterization of colloidal ZnO nanoparticles using nanosecond laser ablation in water, *Appl. Nanosci.*, 1 (2011) 45–49. <https://doi.org/10.1007/s13204-011-0006-3>
- [14] X. Hu et al., Influences of target and liquid media on morphologies and optical properties of ZnO nanoparticles prepared by laser ablation in solution, *J. Am. Ceram. Soc.*, 94 (2011) 4305–4309. <https://doi.org/10.1111/j.1551-2916.2011.04643.x>
- [15] A. M. Mostafa, Preparation and study of nonlinear response of embedding ZnO nanoparticles in PVA thin film by pulsed laser ablation, *J. Mol. Struct.*, 1223 (2021) 129007. <https://doi.org/10.1016/j.molstruc.2020.129007>
- [16] K. Abid, H. Laser, Preparation and Characterization Study of ZnS Thin Films with Different Substrate Temperatures, *Eng. Technol. J.*, 34 (2016) 178–185.
- [17] K. S. Khashan, G. M. Sulaiman, A. H. Hamad, F. A. Abdulameer, A. Hadi, Generation of NiO nanoparticles via pulsed laser ablation in deionised water and their antibacterial activity, *Appl. Phys. A Mater. Sci. Process.*, 123 (2017) 1–10. <https://doi.org/10.1007/s00339-017-0826-4>

- [18] H. H. Bahjat, R. A. Ismail, G. M. Sulaiman, M. S. Jabir, Magnetic Field-Assisted Laser Ablation of Titanium Dioxide Nanoparticles in Water for Anti-Bacterial Applications, *J. Inorg. Organomet. Polym. Mater.*, 31 (2021) 3649–3656. <https://doi.org/10.1007/s10904-021-01973-8>
- [19] N. Yudasari, M. M. Suliyanti, and C. Imawan, Antibacterial activity of Fe-doped ZnO nanoparticles synthesised via pulsed laser ablation in liquid against *Staphylococcus Aureus*, *Adv. Nat. Sci. Nanosci. Nanotechnol.*, 11 (2020). <https://doi.org/10.1088/2043-6254/ab878d>
- [20] S. N. Idris, M. N. Norizan, I. S. Mohamad, N. Mahmed, K. Magiswaran, S. A. Sobri, Synthesis Methods of Tin Oxide as Photoanode for Dye-Sensitized Solar Cell Performance: A Short Review, *Int. J. Nanoelectron. Mater.*, 14 (2021) 199–206.
- [21] M. Pudukudy, Z. Yaakob, Facile Synthesis of Quasi Spherical ZnO Nanoparticles with Excellent Photocatalytic Activity, *J. Clust. Sci.*, 26 (2015) 1187–1201. <https://doi.org/10.1007/s10876-014-0806-1>
- [22] T. Özdal, R. Taktakoğlu, H. Özdamar, M. Esen, D. K. Takçi, H. Kavak, Crystallinity improvement of ZnO nanorods by optimization of low-cost electrodeposition technique, *Thin Solid Films*, 592 (2015) 143–149. <https://doi.org/10.1016/j.tsf.2015.09.013>
- [23] K. L. Menzies, L. Jones, The impact of contact angle on the biocompatibility of biomaterials, *Optom. Vis. Sci.*, 87 (2010) 387–399. <https://doi.org/10.1097/OPX.0b013e3181da863e>